https://ntrs.nasa.gov/search.jsp?R=19910010054 2020-03-19T18:44:25+00:00Z

IN-34
1281
814

NASA Contractor Report 187065

Calculations of Separated 3-D Flows With a Pressure-Staggered Navier-Stokes Equations Solver

(NASA-CR-187065) CALCULATIONS OF SEPARATED 3-D FLOWS WITH A PRESSURE-STAGGERED NAVIER-STOKES EQUATIONS SOLVER Final Report (Texas Univ.) 14 p CSCL 20D G3/34

N91-19367

Unclas 0001281

S.-W. Kim

University of Texas at Arlington
Arlington, Texas

March 1991

Prepared for
Lewis Research Center
Under Cooperative Agreement NCC3-180

National Aeronautics and
Space Administration

CALCULATIONS OF SEPARATED 3-D FLOWS WITH A PRESSURE-STAGGERED NAVIER-STOKES EQUATIONS SOLVER

S. -W. Kim*
University of Texas at Arlington
Arlington, Texas 76010

Summary

A Navier-Stokes equations solver based on a pressure correction method with a pressure-staggered mesh and calculations of separated three-dimensional flows are presented. It is shown that the velocity-pressure decoupling, which occurs when various pressure correction algorithms are used for pressure-staggered meshes, is caused by the ill-conditioned discrete pressure correction equation. The use of a partial differential equation for the incremental pressure eliminates the velocity-pressure decoupling mechanism by itself and yields accurate numerical results. Example flows considered are a three-dimensional lid-driven cavity flow and a laminar flow through a 90° bend square duct. For the lid-driven cavity flow, the present numerical results compare more favorably with the measured data than those obtained using a formally third order accurate quadratic upwind interpolation scheme. For the curved duct flow, the present numerical method yields a grid independent solution with a very small number of grid points, and the calculated velocity profiles are in good agreement with the measured data.

Nomenclature

A_i	coefficient for incremental velocity, (i=u, v, or w)
D_h	hydraulic diameter of the curved duct
(ℓ, m, n)	index for mesh
n_j	outward normal vector, $n_j=\{n_x,n_y,n_z\}$
p	pressure
Re	Reynolds number
r_i	radius of curvature for inner (suction side) wall for curved duct flow
r_o	radius of curvature for outer (pressure side) wall for curved duct flow
u_j	velocity component, $u_j=\{u,v,w\}$
x_j	cartesian coordinates $x_j=\{x,y,z\}$
μ	molecular viscosity of fluid
(ξ,η,ζ)	curvilinear coordinates
Superscripts	
n	iteration count
nb	neighboring grid points; $(\ell+1,m,n)$, $(\ell-1,m,n)$, $(\ell,m-1,n)$, $(\ell,m+1,n)$, $(\ell,m,n-1)$ and $(\ell,m,n+1)$
*	current value
'	incremental (or corrective) value
Subscripts	
i,j	index for spacial coordinates, i={1,2,3} and j={1,2,3}
Mathematical Symbol	
Σ	summation

Introduction

In many flow problems of practical importance, the boundary geometries are complex, and arbitrary shaped blockages may exist inside the flow path. However, an original numerical method based on the SIMPLE algorithm (refs. 1 and 2) has been used to solve incompressible flows whose domain can be discretized using orthogonal meshes. Thus, a number of numerical methods to extend the pressure correction methods for flows with arbitrary geometries have appeared (refs. 3 to 10). Along with the efforts, various pressure correction algorithms (ref. 11) to enhance the convergence nature itself and to increase the convergence rate have also been proposed. A finite volume method to solve the Navier-Stokes equations is presented in this paper. The method is based on a pressure correction method and is valid for both incompressible and compressible flows including Reynolds-averaged Navier-Stokes equations (ref. 12). Calculation of three-dimensional incompressible laminar flows using the method is presented in this paper. Calculations of various two-dimensional flows

*NASA Resident Research Associate at Lewis Research Center.

using the present numerical method can be found in refs. 12 to 14. Example flows considered in these references include: a developing laminar channel flow, a developing laminar pipe flow, a two-dimensional laminar flow through a 90° bend channel, a laminar polar cavity flow and a supersonic flow over a compression ramp with shock wave - turbulent boundary layer interaction.

A number of grid layouts have been proposed and tested to identify the most suitable one to solve the Navier-Stokes equations defined on arbitrary, complex geometries. In Shyy et al. (ref. 3), the standard fully staggered mesh is used to solve the Navier-Stokes equations defined on curved geometries. This grid layout can not be used to solve flows inside a 90° bend duct; see Malisika and Raithby (ref. 5) for more details. In reference 5, the standard fully staggered mesh is extended in such a way that the three velocity components are located at all grid points except at the pressure grid point. In this case, the number of degrees of freedom for velocity is tripled while the degrees of freedom for pressure remains the same as that of the original fully staggered mesh. The accuracy of a numerical method depends not only on the number of velocity grid points but also on the number of pressure grid points. Hence the accuracy can not be improved as much as the tripled velocity degrees of freedom might suggest. A collocated mesh is used in Rhie (ref. 6), Dwyer and Ibrani (ref. 7), Peric et al. (ref. 8) and Majumdar (ref. 9). In reference 6, the velocity-pressure decoupling is prevented by including a fourth order artificial dissipation in the pressure correction equation, while in reference 7, the same purpose is achieved by evaluating the incremental velocities (u',v',w') at mid-sides of the control volume. In Peric et al. (ref. 8) and Majumdar (ref. 9), a velocity-pressure coupled solution is obtained by interpolating the pressure gradient term differently from the other terms in the discrete momentum equation. This method is called as the "momentum interpolation" scheme (ref. 9). Majumdar (ref. 9) showed that the momentum interpolation scheme of Peri et al. (ref. 8) may yield a numerical result that depends on the under-relaxation parameter, and proposed an improved momentum interpolation scheme that yields a unique solution. In Vanka et al. (ref. 10), the velocities are located at the same grid points and the pressure is located at the cetroid of the cell formed by the four adjacent velocity grid points (for the two-dimensional case). The pressure-staggered mesh for the three-dimensional case is shown in figure 1 for clarity in the following discussion. The pressure-staggered mesh was first used in the control volume method by Vanka et al. (ref. 10). They mentioned that it was not easy to obtain convergent solutions due to the velocity-pressure decoupling. The mechanism that leads to the velocity-pressure decoupled solution is heuristically shown in reference 5.

In the present pressure correction algorithm, a partial differential equation for incremental pressure is solved to correct the velocity and pressure field. The mechanism that leads to the velocity-pressure decoupled solution in the pressure-staggered mesh (ref. 10) is identified in the following section, and it is shown that the use of the partial differential equation for incremental pressure eliminates the velocity-pressure decoupling mechanism by itself. The use of the same incremental pressure equation in the collocated mesh also yields a velocity-pressure coupled solution (ref. 15). In the case of an orthogonal, collocated mesh, the present pressure correction scheme becomes very similar to the momentum interpolation scheme (refs. 8 and 9), and both schemes yield strongly diagonally dominant systems of equations for the incremental pressure, see reference 15 for details.

A few pressure correction algorithms, to enhance the convergence nature and to accelerate the convergence rate, have also been proposed and are in use to solve the Navier-Stokes equations. Among these are the SIMPLE-C and the SIMPLE-R (ref. 11). However, it is shown in Jang et al. (ref. 11) that the performance of each pressure correction algorithm (SIMPLE-C or SIMPLE-R) depends somewhat on the particular flow problems to be solved. With any of these methods, the relative error and the mass imbalance can be reduced only to a few orders of magnitude (e.g., 10^{-4}) especially when a highly graded mesh is used. In the present method, solving the partial differential equation for the incremental pressure does not require the use of any specialized pressure correction algorithm. It is shown in the "numerical results" section that the present method yields highly converged results (i.e., the relative error and the mass imbalance are reduced to order of 10^{-8}) within a reasonable number of iterations for the curved duct flow. It can also be found in reference 13 that the relative error can be reduced to the same order for a transonic flow with shock wave - turbulent boundary layer interaction even with the use of a highly stretched mesh (e.g., grid aspect ratio of approximately 100,000).

Numerical Method

The incompressible laminar flow equation are given as;

$$\frac{\partial u_j}{\partial x_j} = 0 \tag{1}$$

$$\frac{\partial}{\partial x_j}\left(\rho u_i u_j\right) - \frac{\partial}{\partial x_j}\left\{\mu\left(\frac{\partial u_i}{\partial x_j} + \frac{\partial u_j}{\partial x_i}\right)\right\} = -\frac{\partial p}{\partial x_i} \tag{2}$$

where the subscripts i and j denote each coordinate direction, and the repeated indices imply summation over the index unless otherwise stated.

In the pressure correction methods, the velocities and the pressure are decomposed as;

$$u_i = u_i^* + u_i' \tag{3}$$

$$p = p^* + p' \tag{4}$$

where the superscript * denotes the current velocities which may not satisfy the conservation of mass equation yet. The discrete momentum equation for u_i-velocity can be written as;

$$A_i(\ell,m,n)u_i(\ell,m,n) = \sum_{nb}\{A_j u_j\} - \frac{\partial p}{\partial x_i} + S_i^v, \quad \text{no sum on i} \tag{5}$$

where A_i is the coefficient of the u_i-velocity at the velocity grid point (l,m,n), S_i^v is the load vector originating from the curvilinear grid structure, the subscript nb denotes the neighboring grid points, and the pressure gradient is left in continuous form deliberately. Substituting equations (3) and (4) into eq. (5) yields;

$$A_i\left(u_i^* + u_i'\right) = \sum_{nb}\left\{A_i\left(u_i^* + u_i'\right)\right\} - \frac{\partial\left(p^* + p'\right)}{\partial x_i} + S_i^v, \quad \text{no sum on i} \tag{6}$$

where the grid point index (ℓ,m,n) has been deleted in equation 6 for convenience. The discrete u_i-momentum equation based on the current flow variables which may not satisfy the conservation of mass equation can be written as;

$$A_i u_i^* = \sum_{nb}\left\{A_i u_i^*\right\} - \frac{\partial p^*}{\partial x_i} + S_i^v, \text{ no sum on i} \tag{7}$$

Subtracting equation (7) from equation (6) yields;

$$u_i' = -\frac{1}{A_i}\frac{\partial p'}{\partial x_i}, \text{ no sum on i} \tag{8}$$

In deriving equation (8), the summation over the neighboring grid points in equations (6) and (7) have been disregarded. Substituting equation (3) into equation (1) yields;

$$\frac{\partial u_j'}{\partial x_j} = -\frac{\partial u^*_j}{\partial x_j} \tag{9}$$

Substituting equation (8) into equation (9) yields the partial differential equation for the incremental pressure given as;

$$\frac{\partial}{\partial x_j}\left\{\frac{1}{A_j}\frac{\partial p'}{\partial x_j}\right\} = -\frac{\partial u_j^*}{\partial x_j} \tag{10}$$

where the last term in equation (10) represents the mass imbalance. Applying the standard finite volume procedure to equation (10) yields the discrete incremental pressure equation. In this case, the value of A_j at the interface of the pressure control volumes is obtained by averaging the A_j values defined at the four adjacent velocity grid points (fig. 1(c)). As all the central-differenced finite volume equations for diffusion equations are strongly diagonally dominant, the present discrete pressure correction equation is strongly diagonally dominant. The momentum interpolation scheme (ref. 8) may yield a numerical result that depends on the under-relaxation parameter (ref. 9). On the other hand, the present pressure correction scheme does not yield a numerical result that depends on the under-relaxation parameter. The pressure correction equation, (eq. (10)), clearly states that the incremental pressure is driven only by the mass imbalance.

For clarity, the mechanism that leads to the velocity-pressure decoupled solution, when various pressure correction algorithms (refs. 1, 5 and 10) are applied to the pressure-staggered (or collocated) mesh, is described below. In these pressure correction algorithms, the influencing pressure nodes for each velocity grid point are identified first. In the case of a pressure-staggered mesh, it is argued that the velocity at a velocity grid point is influenced by the eight adjacent pressure grid points, see figure 1(b). The pressure gradient at the interface of the pressure control volumes is obtained by a veraging the pressure gradients at the four adjacent velocity grid points, see figure 1(c), and that of each velocity grid point is given as:

$$\frac{\partial p'}{\partial x_i} = \frac{\partial p'}{\partial \xi_j}\frac{\partial \xi_j}{\partial x_i} \tag{11}$$

where, for example,

$$\begin{aligned}\frac{\partial p'}{\partial \xi} = &\left\{p'\left(\ell+\frac{1}{2},m-\frac{1}{2},n-\frac{1}{2}\right)+p'\left(\ell+\frac{1}{2},m-\frac{1}{2},n+\frac{1}{2}\right)\right.\\ &\left.+p'\left(\ell+\frac{1}{2},m+\frac{1}{2},n-\frac{1}{2}\right)+p'\left(\ell+\frac{1}{2},m+\frac{1}{2},n+\frac{1}{2}\right)\right\}/4\\ &-\left\{p'\left(\ell-\frac{1}{2},m-\frac{1}{2},n-\frac{1}{2}\right)+p'\left(\ell-\frac{1}{2},m-\frac{1}{2},n+\frac{1}{2}\right)\right.\\ &\left.+p'\left(\ell-\frac{1}{2},m+\frac{1}{2},n-\frac{1}{2}\right)+p'\left(\ell-\frac{1}{2},m+\frac{1}{2},n+\frac{1}{2}\right)\right\}/4\end{aligned} \tag{12}$$

The discrete pressure correction equation is obtained by substituting equations (8) and (11) into equation (9) and integrating it over the pressure control volume. This discrete pressure correction equation contains 27 entries inter-connecting 27 adjacent pressure grid points (for the three-dimensional case) and is not diagonally dominant in general. For uniform flow with uniform mesh, the diagonal entry of this pressure correction equation vanishes, and thus the mass imbalance for a particular pressure grid point tends to correct only the pressure of the adjacent pressure grid points. The velocity-pressure decoupling occurs in such a case, and a convergent solution can not be obtained. On the other hand,

the discrete pressure correction equation, obtained by applying the standard finite volume procedure to equation (10), is strongly diagonally dominant even for highly skewed mesh. For uniform flows, all the off-diagonal entries of the pressure correction equation vanish and only 7 diagonal entries remain in the present pressure correction algorithm, and this discrete equation is strongly diagonally dominant. The rest of the numerical procedures are briefly described below.

The power law upwind differencing scheme (ref. 1) is used for the momentum equation. The pressure gradient in the momentum equation is evaluated using equation (11) with the incremental pressure replaced by the pressure. The current flow velocities are obtained by solving equation (10) with the mass imbalance evaluated from the current velocities. The velocity corrections are obtained using equation (8) and incremental pressure. The velocity and pressure are corrected using equations (3) and (4), and the corrected velocities and pressure are used to obtain new current velocities. The systems of discrete incremental pressure equations and the discrete momentum equations are solved by the Tri-Diagonal-Matrix-Algorithm (ref. 2). The systems of equations are solved iteratively until the residuals become smaller than the prescribed convergence criteria. Each iteration consists of 3 sweeps for the momentum equation and 7 sweeps for the pressure correction equation in each coordinate direction, respectively. The convergence parameters used are;

$$R_1 = \sum_{NC} \left| \frac{\partial u_j}{\partial x_j} \right| \qquad (12a)$$

$$R_2 = \mathrm{Max}\left\{ \mathrm{Max}\left\{ \left| \frac{\left(a_{k,\ell}^{n+1} - a_{k,\ell}^{n}\right)}{A_k^{n+1}} \right| \text{for } \ell = 1,N \right\} \times \text{for } k = (u,v,w,p) \right\} \qquad (12b)$$

where N_c is the number of pressure control volumes; the subscript k denotes each flow variable; the subscript ℓ denotes each grid point; N denotes the number of grid points; and A_k^{n+1} denotes the maximum magnitude of the k-th flow variable at (n+1)th iteration. The iteration is terminated if either equation (12(a)) or equation (12(b)) becomes smaller than the prescribed convergence criterion.

Numerical Results

The numerical method described in the previous sections is tested and evaluated by solving a three-dimensional lid-driven cavity flow (ref. 16) and a laminar flow through a 90° bend square duct (ref. 17).

Lid-Driven Cavity Flow

The lid-driven cavity flow is schematically shown in figure 2. The cavity flow at Reynolds number (based on the transverse velocity, v, and the length of the lid) 3200 is considered in this paper. The flow domain is discretized by 48x35x35 and 78x67x67 meshes in x-, y-, and z-coordinate directions, respectively. The convergence criterion used is 1.0×10^{-4}. The residuals at the time of convergence are $R_1=8.0\times10^{-3}$ and $R_2=1.0\times10^{-4}$, respectively. The calculated transverse velocity (v) profiles on the symmetric plane at y=0.075 m are compared with the measured data (ref. 16) and the numerical results by Freitas et al. (ref. 18) in figure 3(a). It is shown in the figure that the present fine mesh result compare more favorably with the measured data than the one calculated by Freitas et al. (ref. 18) using a formally third order accurate quadratic upwind interpolation scheme. The calculated vertical velocity (w) profiles on the symmetric plane at z=0.075 m are shown in figure 3(b). Again, the present fine mesh result compares more favorably with the measured data than that by Freitas et al. (ref. 18) as shown in the figure.

Laminar Flow Through a 90° Bend Square Duct

The laminar flow through a 90° bend square duct is schematically shown in figure 4. The Reynolds number based on the hydraulic diameter of the duct (D_h=0.04 m) and the bulk velocity is approximately 800. The measured data can be found in Humphrey et al. (ref. 17). Both grid and flow domain independence studies are made for this flow. In the first case, the upstream boundary is located at $4D_h$ upstream of the curved section and the exit boundary is located at $10D_h$ downstream of the curved section. The symmetric half of the flow domain is discretized by 68x18x33 and 110x38x61 meshes in x-, y-, and z-coordinate directions, respectively. In the second case, the upstream boundary is located at $10D_h$ upstream of the curved section, and the symmetric half of the flow domain is discretized by a 92x18x33 grid points in x-, y-, and z-coordinate directions, respectively. In each case, the velocity profile of a fully developed square duct flow is prescribed at the inlet boundary and the vanishing gradient boundary condition is used at the exit boundary. The numerical results obtained using the smaller flow domain are presented below.

The convergence history for the 110x38x61 mesh is shown in figure 5. It is shown in the figure that the converged solution is obtained in approximately 800 iterations. In the finite volume methods, the discrete system of equations is derived by integrating the governing differential equations over the control volume (ref. 1). For flows with arbitrary geometries, the number of interpolations to obtain flow variables at the cell boundaries for the present pressure-

staggered mesh is as small as that of any other grid layout discussed previously. The enhanced convergence rate is partly attributed to the grid layout which requires fewer interpolations.

The calculated longitudinal velocity profiles are shown in figure 6. The present numerical results obtained using the coarse mesh are almost the same as those obtained using the fine mesh which has approximately twice as many grid points in each coordinate direction. The difference between the two sets of present numerical results is less than a few percents in most of the flow domain, which shows that the present numerical method yields an almost grid independent solution with as small as 68x18x33 grid points in the x-, y-, and z-coordinate directions, respectively. It is also shown in the figure that the calculated secondary peaks of the longitudinal velocity near the inner wall ($r=r_i$) are in good agreement with the measured data. It is shown later that such secondary peaks are formed by the secondary fluid motion.

The calculated pressure distributions on the inner and outer walls at the symmetric plane are shown in figure 7, where s is the distance measured along the center line of the duct and s=0 at $\theta=0°$. It can be seen in the figure that the present numerical results are in good agreement with those obtained by Humphrey et al. (ref. 17). The projected velocity vectors on a plane very close to the outer wall ($\zeta=0.005D_h$) are shown in figure 8(a) and the pressure distribution on the same plane is shown in figure 8(b). The plane is located so close to the wall that the velocity component normal to the plane is by far smaller than the velocity component in the figure. It can be seen in these figures that the velocity vectors are aligned in the direction of decreasing pressure, which shows that the fluid motion in the region very close to the wall is governed mostly by the pressure distribution. Due to the strong adverse pressure gradient, a small reversed flow region is formed near the corner wall and the reversed flow region extends up the $\theta\approx37°$ as can be seen in figure 8(a). The projected velocity vectors and the pressure distribution on a plane very close to the side wall ($\eta=0.005D_h$) is shown in figure 9. Again, the velocity component normal to the plane is negligible, and thus the fluid motion in the near-wall region is mostly governed by the pressure distribution. The small reversed flow region near the corner wall, caused by the strong adverse pressure gradient, can also be seen in figure 9(a).

The secondary fluid motions and the pressure distributions at four cross-sections of the curved duct are shown in figure 10. At the inlet of the curved section, figure 10(a), the fluid particle moves upward and recirculatory (or vortex) motion has not been formed yet. On the other hand, the numerical results in Humphrey et al. (ref. 17) show that the recirculatory motion already exists in the same region. To clarify any possible dependence of the numercial results on the location of the inlet boundary, the same flow field is calculated with the inlet boundary located at $10D_h$ upstream of the curved section. The numerical results obtained using the larger flow domain are practically identical to the one shown in figure 10(a). It can be seen in these figures that the recirculatory motion becomes stronger as the fluid particle travels in the downstream direction and that the pressure decreases almost uniformly from the outer (pressure side) wall toward the inner (suction side) wall. These results indicate that the secondary fluid motion is more strongly governed by the strains caused by the streamline curvature than by the pressure distribution. It can also be found from these figures that the secondary peaks of the longitudinal velocity, see figure 6, are caused by the mass carried toward the inner wall by the secondary motion of the fluid.

Conclusions and Discussion

A finite volume method to solve the Navier-Stokes equations and calculations of a three-dimensional lid-driven cavity flow and a laminar flow through 90° bend square duct are presented. A partial differential equation for the incremental pressure and the pressure-staggered mesh form the basis of the present numerical method.

The use of various pressure correction algorithm (refs. 1, 5 and 10) for pressure-staggered mesh yields ill-conditioned discrete pressure correction equation, and the velocity-pressure decoupling is caused by the ill-conditioned discrete pressure correction equation. For example, the diagonal entry of the discrete pressure correction equation obtained by applying various pressure correction algorithms (refs. 1, 5 and 10) vanishes for a uniform flow, with the flow domain discretized uniformly using the pressure-staggered mesh. In such case, the mass imbalance at a particular pressure node corrects only the pressure of the adjacent pressure grid points, and a converged solution can not be obtained. On the other hand, the use of a partial differential equation for incremental pressure yields a strongly diagonally dominant discrete pressure correction equation even when highly graded and skewed mesh is used to discretize the flow domain (ref. 13), and it also yields a unique solution. The present method can also be extended to solve compressible flows by including convective incremental pressure terms into the pressure correction equation (ref. 13).

The use of the same incremental pressure equation in the collocated mesh yields a velocity-pressure coupled solution even though the resulting numerical method is not as strongly convergent as the present method adopting the pressure-staggered mesh. The pressure-staggered mesh is preferred over the collocated mesh for its strongly convergent nature, and is also preferred over the other grid layouts (ref. 5) for its compactness. As a remark, the present pressure correction scheme becomes very similar to the momentum interpolation scheme (refs. 8 and 9) in the case of an orthogonal, collocated mesh (ref. 15). Even in this case, the present pressure correction algorithm yields a unique solution without the use of a specialized interpolation scheme as the one proposed by Majumdar (ref. 9).

In the region very close to the bottom wall of the lid-driven cavity, the transverse velocity (v) obtained using the

quadratic upwind interpolation scheme (ref. 18) compares more favorably with the measured data than the present numerical result. However, in most of the flow region, the present numerical results compare more favorably with the measured data than the other numerical results (ref. 18). A similar situation can be found in a lid-driven polar cavity flow for which the numerical results obtained using the present method compare more favorably with the measured data than those obtained using a second order differencing scheme (ref. 12). These observations indicate that correctly resolving the pressure field is as important as, or more important than, using a higher order differencing scheme.

It is shown that the present numerical method yields a grid independent solution for the curved duct flow with a very small number of grid points. It is also shown that the method yields a rapidly convergent solution for the fine mesh case. The mass imbalance decreases approximately eight orders of magnitude within a reasonable number of iterations for the fine mesh case. These errors are a few orders of magnitude smaller than those obtainable using various other pressure correction algorithms (ref. 11), especially when a fine mesh is used to discretize the flow domain. Such an improved convergence nature is also attributed to the present pressure correction algorithm. The domain independence study shows that the numerical results obtained with the inlet boundary located at $10D_h$ upstream of the curved section are practically identical to those obtained with the inlet boundary located at $4D_h$ upstream of the curved section. Both numerical results show that the recirculatory motion has not been formed at the inlet of the curved section, while the numerical results of Humphrey et al. (ref. 17) shows such a recirculatory motion at the same location. At further downstream locations, the present numerical method predicts a stronger secondary flow motion than that of Humphrey et al. (ref. 17) does. The present numerical results are in very good agreement with the measured data and indicate that the secondary peak of the longitudinal velocity is formed by the mass carried toward the inner wall by the secondary motion of the fluid.

References

1. Patankar, S.V.; and Shih, T.M.: Numerical Heat Transfer and Fluid Flow. McGraw-Hill, New York, 1980.
2. Gosman, A.D.; and Ideriah, F.J.K.: TEACH -T. Department of Mechanical Engineering, Imperial College, London, 1982.
3 Shyy, W.; Thong, S.S.; and Corea, S.M.: Numerical Recirculating Flow Calculation Using a Body-Fitted Coordinate System. Numer. Heat Trans., vol. 8, no.1, 1985, pp.99-113.
4. Karki, K.C.; and Patankar, S.V.: A Pressure Based Calculation Procedure for Viscous Flows at All Speeds in Arbitrary Configurations. AIAA J., vol. 27, no. 9, Sept. 1989, pp.1167-1174.
5. Maliska, C.R.; and Raithby, G.D.: A Method for Computing Three Dimensional Flows Using Non-Orthogonal Boundary-Fitted Coordinates. Int. J. Numer. Methods Fluids, vol. 4, 1984, pp.519-537.
6. Rhie, C.M.: A Pressure Based Navier-Stokes Solver Using the Multigrid Method. AIAA Paper 86-0207, Jan. 1986.
7. Dwyer, H.A.; and Ibrani, S.: Time Accurate Solutions of the Incompressible and Three-Dimensional Navier-Stokes Equations. AIAA Paper 88-0418, Jan. 1988.
8. Peric, M.; Kessler, R.; and Scheuerer, G.: Comparison of Finite-Volume Numerical Methods with Staggered and Colocated Grids. Computers Fluids, vol. 16, no. 4, 1988, pp.389-403.
9. Majumdar, S.: Role of Underrelaxation in Momentum Interpolation for Calculation of Flow with Nonstaggered Grids. Numer. Heat Trans., vol. 13, no.1, 1988, pp.125-132.
10. Vanka,S.P.; Chen, B.C.J.; and Sha, W.T.: A Semi-Implicit Calculation Procedure for Flows Described in Boundary Fitted Coordinate Systems. Numer. Heat Trans., vol. 3, Jan-Mar. 1980, pp.1-19.
11. Jang, D.S.; Jetli, R.; and Acharya, S.: Comparison of the PISO, SIMPLER, and SIMPLEC Algorithms for the Treatment of the Pressure-Velocity Coupling in Steady Flow Problems. Numer. Heat Trans., vol. 10, no. 3, 1986, pp.209-228.
12. Kim, S.-W.: A Control-Volume Based Navier-Stokes Equation Solver Valid at All Flow Velocities. NASA TM-101488, 1989.
13. Kim, S.-W.: Numerical Investigation of Separated Transonic Turbulent Flows with a Multiple-Time-Scale Turbulence Model. Numer. Heat Trans., Part A, vol. 18, no.2, 1990, pp.149-171.
14. Kim, S.-W.: Calculation of Reattaching Shear Layers in Divergent Channel with a Multiple-Time-Scale Turbulence Model. AIAA Paper 90-0047, Jan. 1990 (Also, NASA TM-102293).
15. Kim, S.-W.: On the Anomaly of Velocity-Pressure Decoupling in Collocated Mesh. NASA TM, In print, 1991.
16. Koseff, J.R.; and Street, R.L.: The Lid-Driven Cavity Flow: A Synthesis of Qualitative and Quantitative Observations. J. Fluids Eng., vol. 106, no.4, 1984, pp.390-398.
17. Humphrey, J.A.C.; Taylor, A.M.K.; and Whitelaw, J.H.: Laminar Flow in a Square Duct of Strong Curvature. J. Fluid Mech., vol. 83, pt. 3, Dec.5, 1977, pp.509-527.
18. Freitas,C.J.; et al.: Numerical Simulation of Three-Dimensional Flow in a Cavity. Int. J. Numer. Methods Fluids, vol. 5, 1985, pp.561-575.

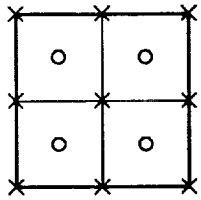

(a) 2-D projection of pressure-staggered mesh.

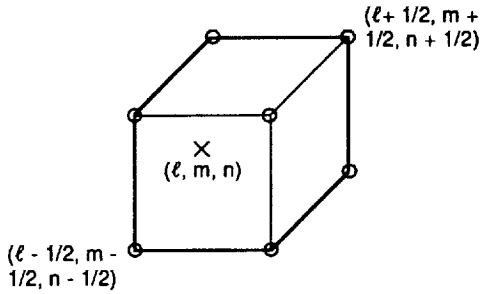

(b) Control volume for velocity.

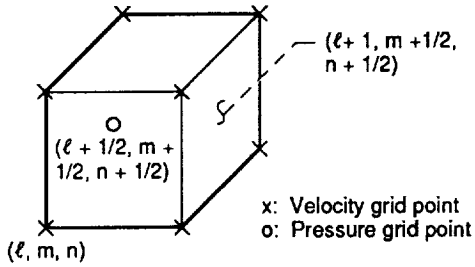

(c) Contol volume for pressure.

Figure 1.—Pressure staggered mesh.

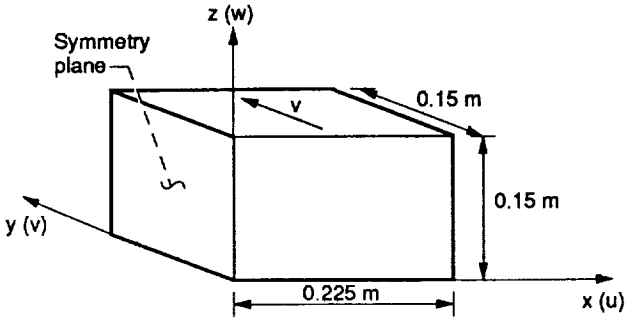

Figure 2.—Lid driven cavity flow.

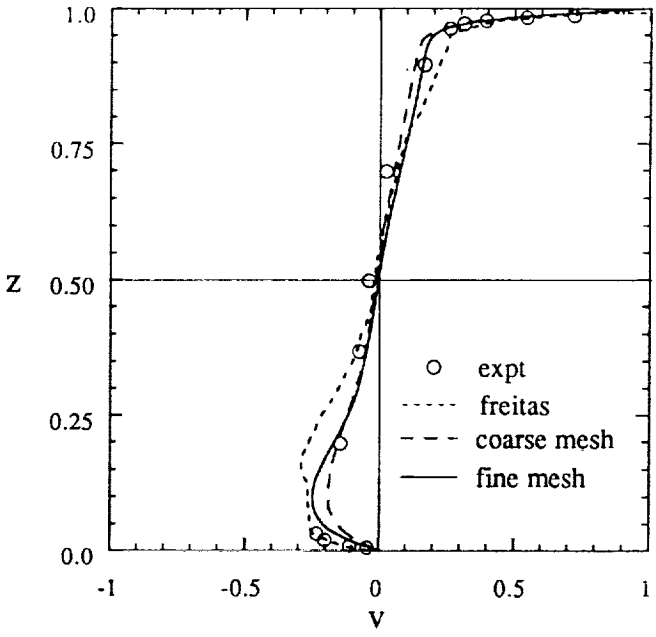

(a) Transverse velocity on symmetric plane (y = 0.075 m).

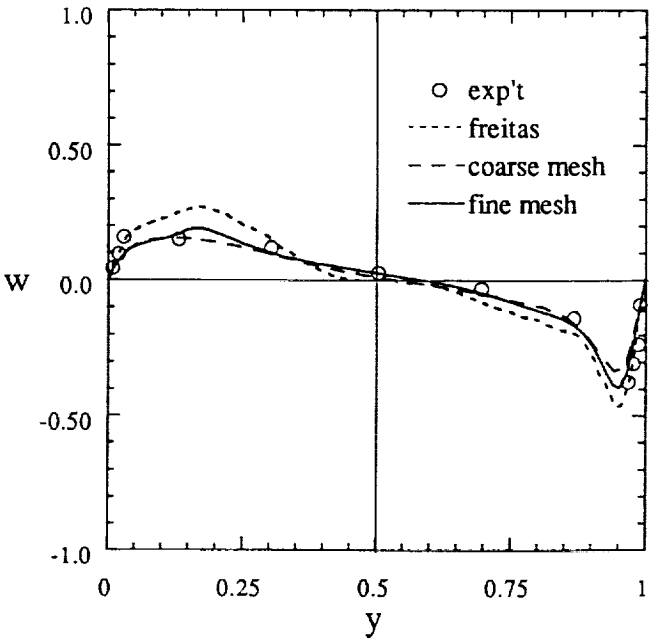

(b) Vertical velocity on symmetric plane (z = 0.075 m).

Figure 3.—Velocity profiles for cavity flow.

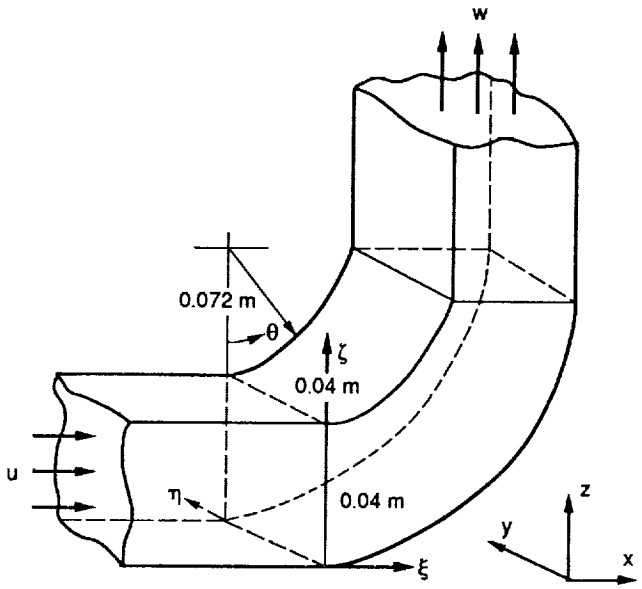

Figure 4.—Laminar flow through a 90° bend square duct.

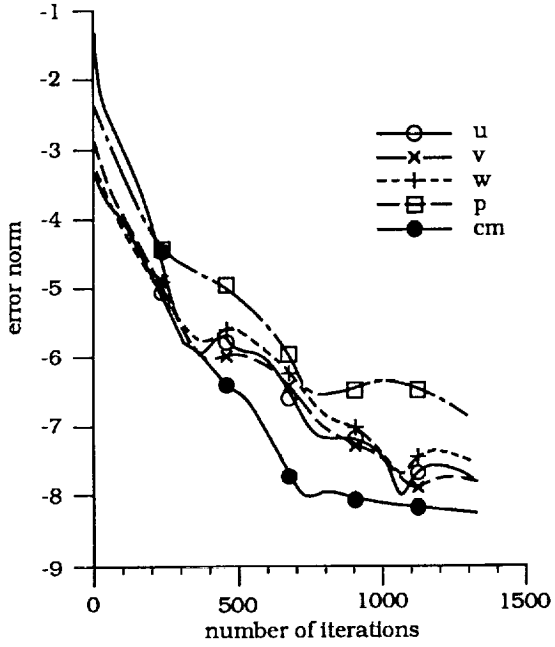

Figure 5.—Convergence history, (u, v, w, p: relative error; cm: L_2 norm of conservation of mass).

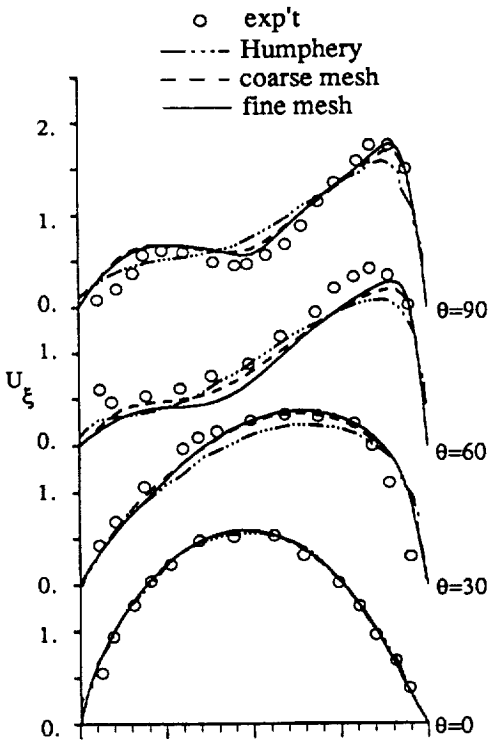

(a) On symmetric plane (y/D_h = 0.5).

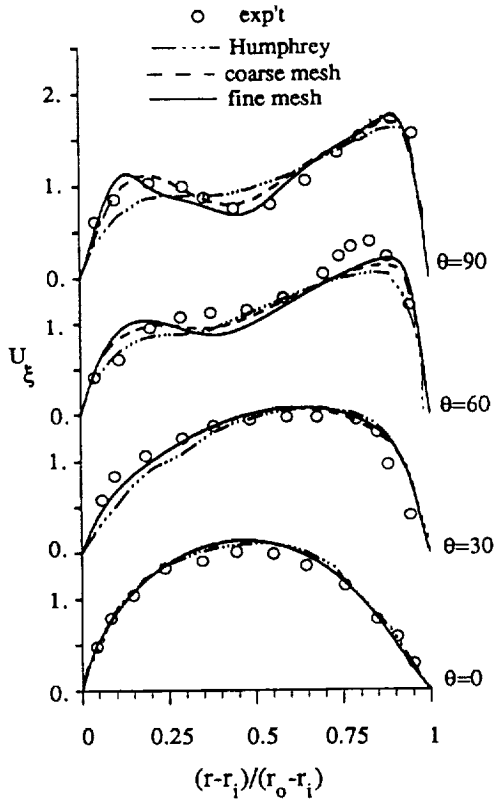

(b) On quarter plane (y/D_h = 0.25).

Figure 6.—Velocity profiles for curved duct flow.

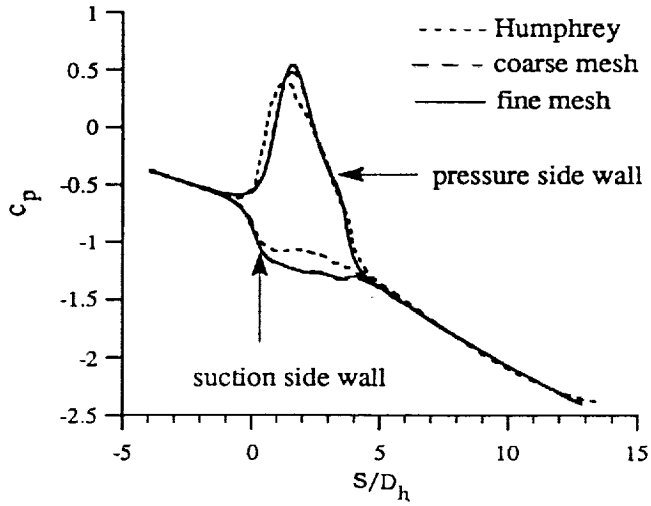

Figure 7.—Pressure distributions on the wall.

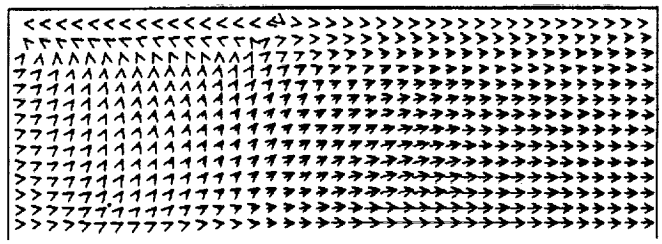

(a).

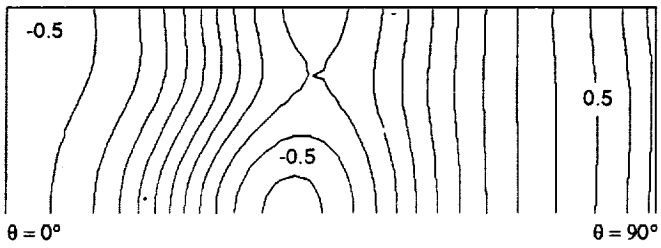

(b).

Figure 8.—Velocity vector and pressure contour on (ξ, η) plane at $\zeta/D_h = 0.005$.

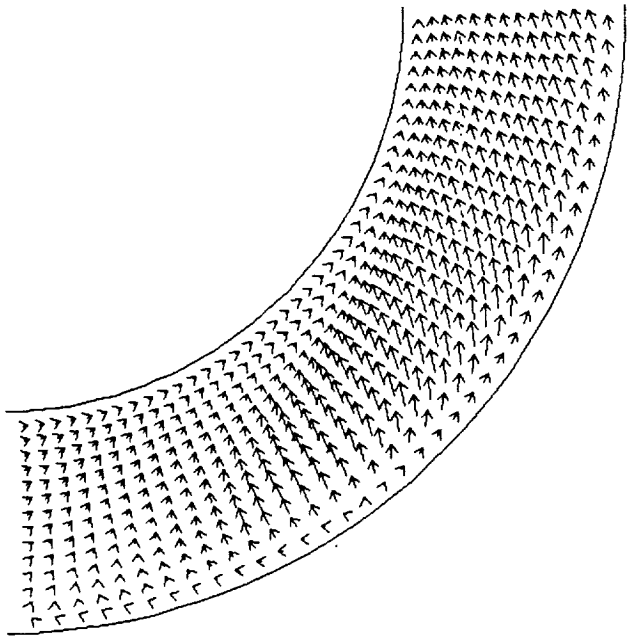

(a).

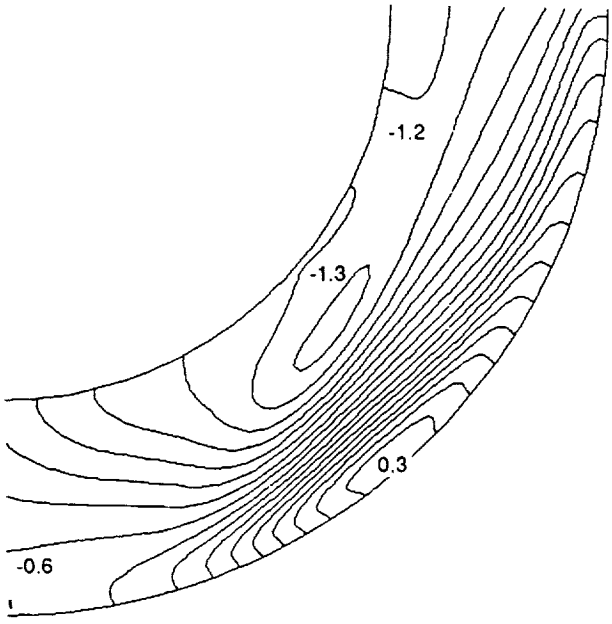

(b).

Figure 9.—Velocity vector and pressure contour on (ξ, ζ) plane at $\eta/D_h = 0.005$.

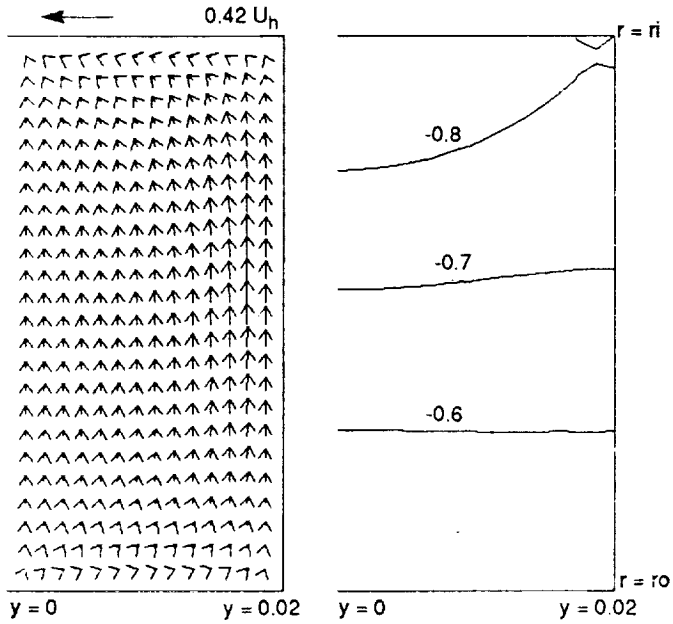

(a) θ = 0°.

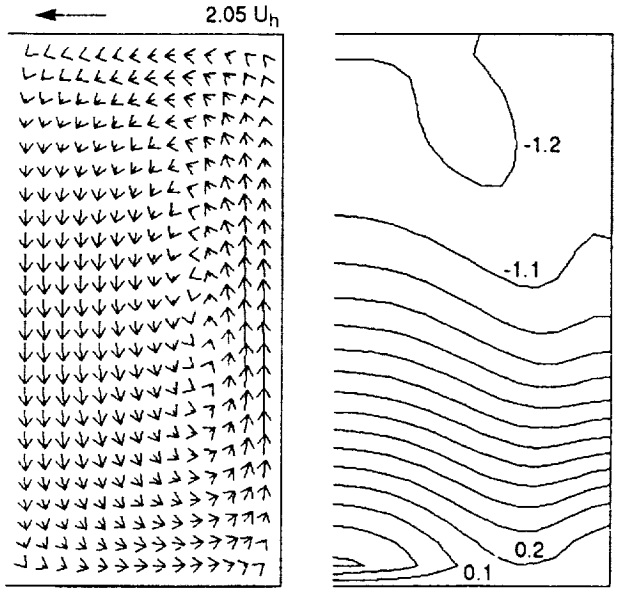

(b) θ = 30°.

Figure 10.—Secondary velocity vector and pressure contour.

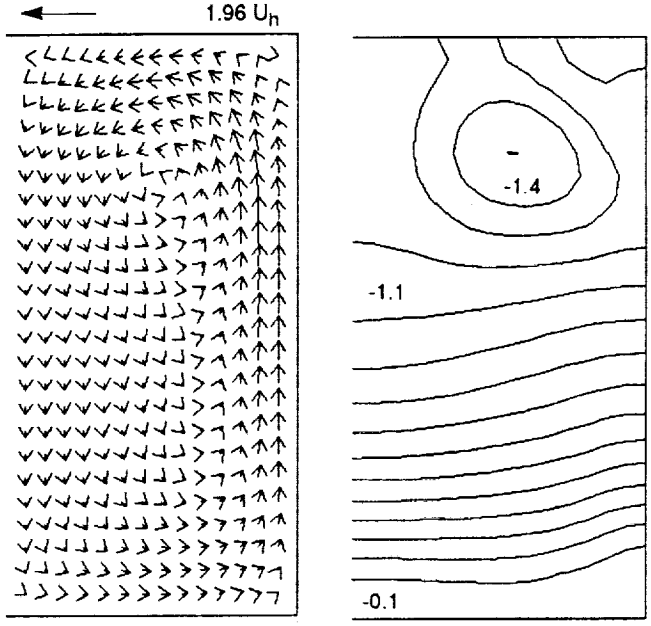

(c) $\theta = 60°$.

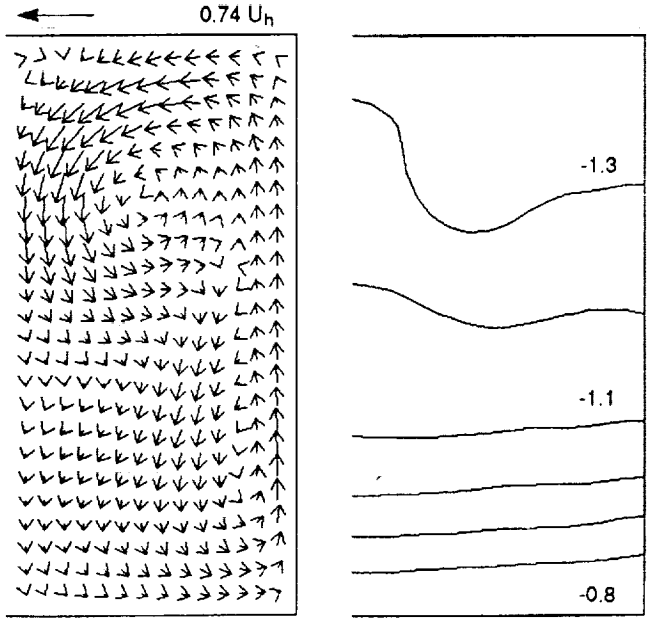

(d) $\theta = 90°$.

Figure 10.—Concluded.

NASA
National Aeronautics and Space Administration

Report Documentation Page

1. Report No.	2. Government Accession No.	3. Recipient's Catalog No.
NASA CR-187065		

4. Title and Subtitle	5. Report Date
Calculations of Separated 3-D Flow With a Pressure-Staggered Navier-Stokes Equations Solver	March 1991
	6. Performing Organization Code
7. Author(s)	8. Performing Organization Report No.
S.-W. Kim	None (E-5988)
	10. Work Unit No.
	505-62-52
9. Performing Organization Name and Address	11. Contract or Grant No.
University of Texas at Arlington Arlington, Texas 76010	NCC3-180
	13. Type of Report and Period Covered
	Contractor Report Final
12. Sponsoring Agency Name and Address	14. Sponsoring Agency Code
National Aeronautics and Space Administration Lewis Research Center Cleveland, Ohio 44135-3191	

15. Supplementary Notes

Project Manager, Robert Stubbs, Internal Fluid Mechanics Division, NASA Lewis Research Center. S.-W. Kim, NASA Resident Research Associate at Lewis Research Center.

16. Abstract

A Navier-Stokes equations solver based on a pressure correction method with a pressure-staggered mesh and calculations of separated three-dimensional flows are presented. It is shown that the velocity-pressure decoupling, which occurs when various pressure correction algorithms are used for pressure-staggered meshes, is caused by the ill-conditioned discrete pressure correction equation. The use of a partial differential equation for the incremental pressure eliminates the velocity-pressure decoupling mechanism by itself and yields accurate numerical results. Example flows considered are a three-dimensional lid-driven cavity flow and a laminar flow through a 90 degree bend square duct. For the lid-driven cavity flow, the present numerical results compare more favorably with the measured data than those obtained using a formally third order accurate quadratic upwind interpolation scheme. For the curved duct flow, the present numerical method yields a grid independent solution with a very small number of grid points, and the calculated velocity profiles are in good agreement with the measured data.

17. Key Words (Suggested by Author(s))	18. Distribution Statement
Navier-stokes equation Pressure-staggered mesh Cavity flow Curved duct flow	Unclassified – Unlimited Subject Category 34

19. Security Classif. (of this report)	20. Security Classif. (of this page)	21. No. of pages	22. Price*
Unclassified	Unclassified	14	A03

*For sale by the National Technical Information Service, Springfield, Virginia 22161